Available online at www.sciencedirect.com

SciVerse ScienceDirect

Ceramics International 39 (2013) 7241–7246

CERAMICS INTERNATIONAL

www.elsevier.com/locate/ceramint

Short communication

# High dielectric loss and microwave absorption behavior of multiferroic $BiFeO_3$ ceramic

Jie Yuan[a], Zhi-Ling Hou[b], Hui-Jing Yang[a], Yong Li[a], Yu-Qing Kang[a], Wei-Li Song[a], Hai-Bo Jin[a], Xiao-Yong Fang[a], Mao-Sheng Cao[a,*]

[a]*School of Materials, Beijing Institute of Technology, Beijing 100081, PR China*
[b]*School of Science, Beijing University of Chemical Technology, Beijing 100029, PR China*

Received 30 December 2012; received in revised form 11 January 2013; accepted 22 January 2013
Available online 30 January 2013

**Abstract**

Single-phase multiferroic $BiFeO_3$ nanoparticles were synthesized by the sol–gel method. Their dielectric properties are investigated in the temperature range of 373–773 K at frequencies 12.4–18 GHz. Multiferroic $BiFeO_3$ shows high dielectric loss and a strong positive temperature dependence of dielectric properties. The average real and imaginary permittivities of BFO increase from 15.5 and 5.5 to 21.8 and 11.4, respectively. The high dielectric loss below 773 K is ascribed to the defect relaxation loss rather than the leakage current conventionally considered. The calculated attenuation results suggest that BFO nanoparticle is a promising microwave absorber at high temperatures.


*Keywords:* C. Dielectric properties; $BiFeO_3$ ceramic; Microwave absorption

## 1. Introduction

Multiferroic materials, which combine ferromagnetic and ferroelectric features, have attracted much attention because of their potential applications in data storage, spin valves, quantum electromagnets, and microelectronic devices [1–6]. Perovskite-type $BiFeO_3$ (BFO) is the most important room-temperature multiferroic material due to its high ferroelectric Curie temperature ($T_C \sim 1103$ K)[7] and G-type anti-ferromagnetic Néel temperature ($T_N \sim 647$ K), [8] which are beneficial for many applications. However, the macroscopic magnetization of BFO is canceled, and the observation of linear magneto-electric effects is inhibited, due to the combined spatially modulated spiral spin structure with an incommensurate wavelength of $\lambda \sim 62$ nm [9]. Moreover, the low resistivity of BFO is another problem because of oxygen non-stoichiometry. Therefore, BFO could not be exploited for any novel application. Many attempts have been made to resolve these problems, including the synthesis of single phase BFO [10], cation doping [11–16], and forming solid solutions with other materials [17–20]. Recently, intensive research has focused on the dielectric properties, electromagnetic interference shielding, and microwave absorption at GHz frequencies to protect the environment and sensitive circuits from radiation emitted from telecommunication apparatuses [21–24]. In particular, the dielectric properties of BFO material in the GHz region have also attracted considerable interest [25–27]. BFO may be a possible candidate for potential high-temperature microwave applications due to its high Curie temperature and high Néel temperature. However, little literature has been reported on the high-temperature dielectric property of BFO at GHz, while the study of BFO has become more significant on microwave applications.

In this study, we report the dielectric properties of multiferroic BFO nanoparticles in the range of 12.4–18 GHz (the Ku band) at high temperatures from 293 to 773 K. It was found that the BFO exhibited high dielectric loss and a strong positive temperature dependence of its dielectric properties at

*Corresponding author. Tel.: +86 10 68914062.
*E-mail address:* caomaosheng@bit.edu.cn (M.-S. Cao).

0272-8842/$ - see front matter © 2013 Elsevier Ltd and Techna Group S.r.l. All rights reserved.
http://dx.doi.org/10.1016/j.ceramint.2013.01.068

the frequencies investigated, and the origin of the observed dielectric relaxations is discussed.

## 2. Experimental procedure

The BFO nanoparticles were synthesized by the sol–gel method. Bismuth nitrate ($Bi(NO_3)_3 \cdot 5H_2O$) and iron nitrate ($Fe(NO_3)_3 \cdot 9H_2O$) in suitable stoichiometric proportions were dissolved in 2-methoxyethanol ($C_3H_8O_2$). Appropriate amount of citric acid and 2-methoxyethanol was used to adjuste the pH of the solution to about 4, and polyethylene glycol was subsequently added as a dispersant. The mixture was stirred for 30 min at 50 °C to form the sol. The sol was dried at 80 °C for 48 h to form a dried gel. This gel was calcined at 300 °C and then sintered at 500 °C for 2 h to form the product.

The structure and morphology of the BFO nanoparticles were investigated by X-ray diffraction (XRD, X'Pert PRO, Cu-$K_\alpha$) and high-resolution transmission electron microscopy (HRTEM, JEM-2010). For the measurements of DC conductivity, the BFO powders were pressed into pellets with a diameter of 10 mm and a thickness of 0.74 mm. The DC conductivity measurements of BFO nanoparticles were carried out using an Agilent 34970A multi-meter. For measurements of the dielectric properties, the BFO powders were pressed into pellets with dimensions of 15.20 mm × 7.56 mm × 2.26 mm and then annealed at 500 °C for 30 min. The complex permittivity (real part $\varepsilon'$ and imaginary part $\varepsilon''$) of BFO nanoparticles was assessed on a vector network analyzer (ANRIGSU 37269D) using a test apparatus described elsewhere [28].

## 3. Results and discussion

Fig. 1(a) shows a typical TEM image of the as-prepared nanoparticles. It is observed that the samples are spherical particles with an apparently slightly rough surface, and the grain size is around 60–120 nm. The XRD patterns of the samples reveal that the nanoparticles are made of highly crystallized BFO, as shown in Fig. 1(d). All the diffraction peaks are perfectly indexed as a rhombohedrally distorted perovskite with space group $R3c$ (No. 161) and lattice parameters $a=5.582(4)$ Å $c=13.876(7)$ Å. There is no evidence of impurity phases in the samples, such as $Bi_2Fe_4O_9$ and $Bi_2O_3$. The high-resolution TEM (HRTEM) image (Fig. 1(b)) shows the clearly resolved crystalline domains with a uniform inter-planar spacing of 0.39 nm, which correspond to the (012) plane of the BFO crystal. Fig. 1(c) shows a selected-area electron diffraction (SAED) pattern of a typical individual particle, which can be indexed to the [42$\bar{1}$] zone axis of BFO. The sharp diffraction spots indicate that BFO nanoparticles were well-developed in a single-crystal structure.

Fig. 2 shows the complex permittivity of BFO in the Ku band at various temperatures. It is observed that, at 293–773 K, both real permittivities $\varepsilon'$ and imaginary permittivities $\varepsilon''$ have a relatively small change at different frequencies.

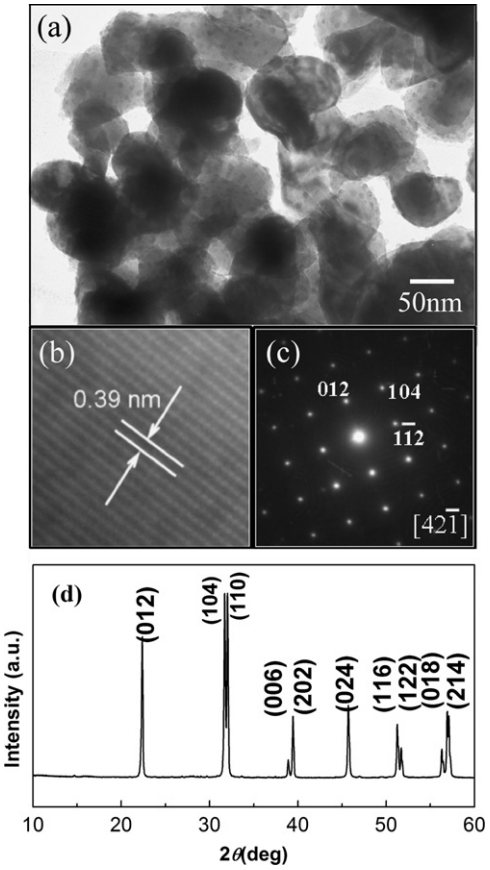


Fig. 1. (a) TEM image, (b) HRTEM image, (c) selected-area electron diffraction (SAED) pattern, and (d) XRD pattern of $BiFeO_3$ nanoparticles.

However, $\varepsilon'$ and $\varepsilon''$ increase obviously with increasing temperature at all the frequencies investigated. The average real and imaginary permittivities of BFO increase from 15.5 and 5.5 to 21.8 and 11.4, respectively. Therefore, $\varepsilon'$ and $\varepsilon''$ depend weakly on frequency, while they rely heavily on temperature. According to the Debye equation, $\varepsilon'$ depends on the polarization relaxation time:

$$\varepsilon'(\omega) = \varepsilon_s' + \frac{\varepsilon_s' - \varepsilon_\infty'}{1+\omega^2\tau^2(T)}, \quad (1)$$

where $\varepsilon_s'$ is the relative static permittivity, $\varepsilon_\infty'$ is the relative optical permittivity, $\omega$ is the angular frequency, and $\tau(T)$ is the temperature-dependent relaxation time, which is the inverse of the angular frequency of maximum dielectric loss. As a large number of oxygen vacancies exist in the crystal structure of BFO [29,30], the relaxation time is dominated by defect relaxation in the Ku band. The defect relaxation time can be expressed as [31]

$$\tau(T) = A\exp\left[\frac{B}{(T-T_0)^{3/2}}\right] \quad (2)$$

where $A$ is the minimum relaxation time (it would reach at an infinite temperature), $B$ is the effective activation energy, and $T_0$ is the Vogel temperature. From Eqs. (1) and (2), it is found that the defect relaxation time decreases with increasing temperature, resulting in an increase in $\varepsilon'$ of BFO.

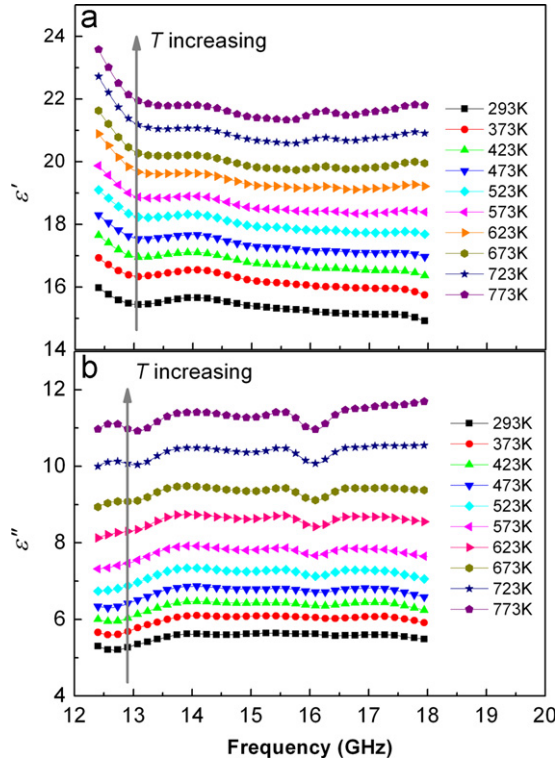


Fig. 2. Frequency dependence of (a) real permittivity $\varepsilon'$ and (b) imaginary permittivity $\varepsilon''$ for $BiFeO_3$ nano-particles at different temperatures (293 K, 373 K, 473 K, 573 K, 673 K, and 773 K).

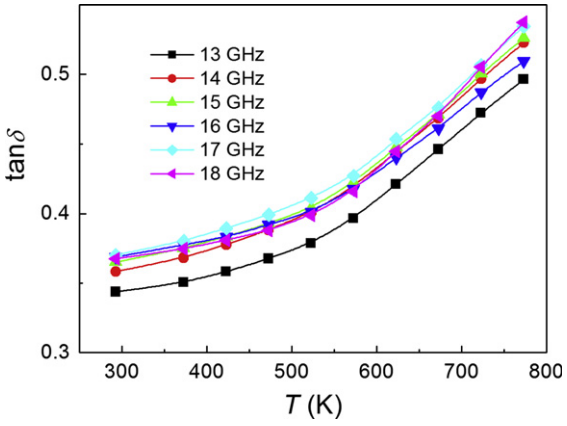


Fig. 3. Temperature dependence of the dielectric loss tangent, tan $\delta$, for $BiFeO_3$ nano-particles.

Fig. 2(b) shows that multiferroic BFO possesses a high dielectric loss in the Ku band, which strongly and positively depends on temperature. Moreover, the change of $\varepsilon''$ is more significant than that of $\varepsilon'$ with the influence of temperature on the loss tangent (tan $\delta$), as is clearly seen in Fig. 3. The magnitude of $\varepsilon''$ can also be expressed in terms of the Debye equation:

$$\varepsilon''(\omega) = \frac{\varepsilon_s' - \varepsilon_\infty'}{1+\omega^2\tau^2(T)}\omega\tau(T) + \frac{\sigma(T)}{\varepsilon_0\omega}, \quad (3)$$

where $\sigma(T)$ is the temperature-dependence leakage conductance and $\varepsilon_0$ is the vacuum permittivity. Thus, $\varepsilon''$ depends on both polarization loss and leakage conductance loss based on Eq. (3). Generally, the leakage current caused by oxygen vacancy is widely considered to be a major influential factor on the high dielectric loss for BFO at GHz frequencies. However, in this study, we suggest that the high dielectric loss of BFO should be primarily dominated by defect relaxation loss rather than leakage conductance loss. The mechanism of dielectric loss in BFO is discussed further.

Fig. 4 shows the plot of DC conductance of BFO at 293–773 K. It is observed that DC conductance slowly increases first and then sharply increases with the rising temperature. Hence, DC conductance is also strongly dependent on temperature in the range 600–773 K, while it is poorly temperature-dependent below 600 K. The DC conductance of BFO can be expressed by [32]

$$\sigma(T) = \sigma_0 \exp\left(-\frac{U}{2kT}\right), \quad (4)$$

where $\sigma_0$ is a pre-exponential factor (the influence of temperature is negligible), $k$ is the Boltzmann constant, and $U$ is equal to the defect ionization energy for oxygen vacancy. According to Eqs. (3) and (4), the fitted curves for $\ln(\sigma(T))$ and $\ln\{\omega\varepsilon_0[\varepsilon''(T)-\varepsilon''(293)]\}$ are shown in the inset of Fig. 4. Since the greatest possibility of a strong influence of leakage conductance on dielectric loss should only occur at high temperature, the points corresponding to temperatures below 600 K were excluded from the fitting procedure. From the inset of Fig. 4, we can conclude that the leakage current originating from oxygen vacancy does not have a dominant influence on the dielectric loss of BFO, due to the difference in the slopes of the fitted curves. Therefore, the high dielectric loss of BFO in the Ku band should be mainly attributed to defect relaxation, which is similar to $\varepsilon'$. It is known that the relaxation time is equal to the inverse of the resonant angular frequency. Thus, the resonant frequency moves toward higher frequencies with increasing temperature, according to Eq. (2). Therefore, we

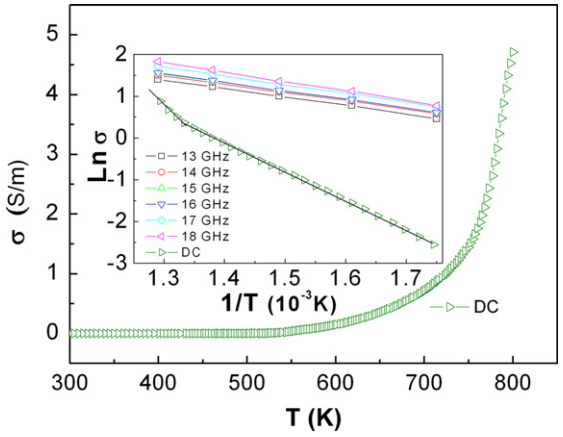


Fig. 4. Temperature dependence of DC conductance for BFO nanoparticles. The inset shows the fitted curves for $\ln[\sigma(T)]$ and $\ln\{\omega\varepsilon_0[\varepsilon''(T)-\varepsilon''(293)]\}$ above 600 K.

can deduce that the resonant frequencies are less than 12.4 GHz in the temperature range because of the positive temperature dependence of relaxation loss.

In order to investigate the high-temperature microwave absorption properties of BFO, we calculate the high-temperature reflection loss at different frequencies. For the microwave-absorption layer on a metal back plane, the reflection loss ($R$) is expressed as [33,34]

$$R = 20\log\frac{|Z_{in}-1|}{|Z_{in}+1|}. \quad (5)$$

Here the normalized input impedance $Z_{in}$ of microwave-absorption layer reads

$$Z_{in} = \sqrt{\frac{\mu_r}{\varepsilon_r}}\tanh\left(j\frac{2\pi fd}{C}\sqrt{\mu_r\varepsilon_r}\right), \quad (6)$$

where $C$ is the velocity of light in vacuum, $f$ is the frequency, $\mu_r$ and $\varepsilon_r$ are the relative permeability and permittivity of the composite medium, respectively, and $d$ is the thickness of microwave-absorption layer. Fig. 5(a) shows the reflection loss of BFO at different frequencies using the complex permittivity and permeability as shown in Fig. 2(a) and (b). All the values were obtained in the same case with the thickness $d$=1.2 mm. It is obviously observed that the maximum absorbing peak decreases and shifts toward lower frequency when the temperature increases. According to the electromagnetic field theory, the maximum attenuation is documented by quarter-wavelength resonance. The

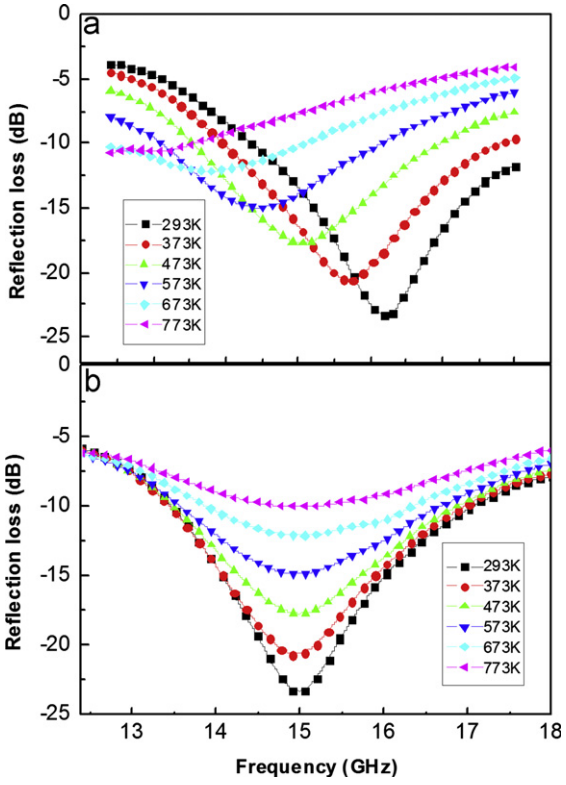


Fig. 5. High-temperature microwave absorption of BFO nanoparticles. (a) Reflection loss at thickness 1.2 mm and (b) Reflection loss at resonant frequency 15 GHz.

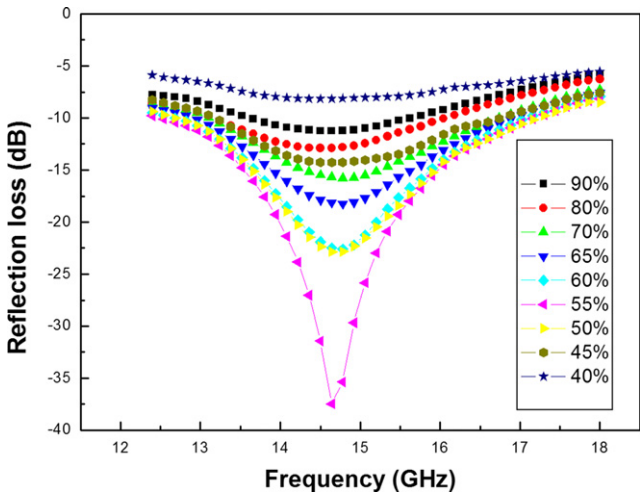


Fig. 6. Reflection loss at temperature 773 K with various densities.

relationship between resonance frequency $f_r$ and thickness can be described by

$$f_r = \frac{C}{4d\times \mathrm{Re}(\sqrt{\mu_r\varepsilon_r})}. \quad (7)$$

Therefore, according to Eq. (7), the resonance frequency shifts toward lower frequency with the increasing $\varepsilon_r$ as temperature increases. Fig. 5(b) shows the high-temperature resonant absorption for BFO (15 GHz) in the temperature range 293–773 K. The maximum absorbing value descends from 23.3 dB at 293 K to 10.1 dB at 773 K. Although the dielectric loss significantly increases with the increase of temperature, a monotonic decrease in the calculated attenuation is observed when the temperature increases. The opposite behavior can be explained by impedance matching conditions. The similar phenomenon has also observed in other absorbing materials, such as CNTs nanocomposites [35].

In order to evaluate the potential ability of microwave absorption at high temperature, we calculate the reflection loss of the samples with various densities at 773 K based on the Bruggeman formula [36], as shown in Fig. 6. It is found that the maximum attenuation occurs around 55% of the theoretical density, which is up to 37 dB. More importantly, the strong attenuation may be achieved in the wide density range from 50% to 60%, which is more than 10 dB in the frequency range 12.7–17 GHz. It is suggested that BFO may be an excellent absorber at high temperature. Therefore, the excellent microwave absorption can be attained through adjusting the complex permittivity by changing BFO materials density or compounding it with low-loss materials.

## 4. Conclusions

The multiferroic $BiFeO_3$ nanoparticles are successfully synthesized by the sol–gel method. High dielectric loss and strong positive temperature dependence are observed in the complex permittivity spectra of BFO nanoparticles in the Ku

band. Although DC conductance shows strong positive temperature dependence, analysis of the results suggests that defect relaxation plays a major role in the high dielectric loss of BFO. The calculated attenuation results show that the maximum absorbing peak decreases and shifts towards lower frequency under the same thickness when the temperature increases, which is resulted from impedance matching and quarter-wavelength resonance, respectively. Consequently, multiferroic BFO materials have great potential to be applied in the field of high temperature microwave absorption.

## Acknowledgment

The authors gratefully acknowledge the National Natural Science Foundation of PR China (Nos. 51132002, 50972014, 51072024 and 51102007).

## References

[1] K.F. Wang, J.M. Liu, Z.F. Ren, Multiferroicity: the coupling between magnetic and polarization orders, Advances in Physics 58 (2009) 321–448.
[2] Y. Tokunaga, N. Furukawa, H. Sakai, Y. Taguchi, T.H. Arima, Y. Tokura, Composite domain walls in a multiferroic perovskite ferrite, Nature Materials 8 (2009) 558–562.
[3] L. Wang, J.B. Xu, B. Gao, A.M. Chang, J. Chen, L. Bian, C.Y. Song, Synthesis of $BiFeO_3$ nanoparticles by a low-heating temperature solid-state precursor method, Materials Research Bulletin 48 (2013) 383–388.
[4] J.X. Zhang, Q. He, M. Trassin, W. Luo, D. Yi, M.D. Rossell, P. Yu, L. You, C.H. Wang, C.Y. Kuo, J.T. Heron, Z. Hu, R.J. Zeches, H.J. Lin, A. Tanaka, C.T. Chen, L.H. Tjeng, Y.H. Chu, R. Ramesh, Microscopic origin of the giant ferroelectric polarization in tetragonal-like $BiFeO_3$, Physical Review Letters 107 (2011) 147602.
[5] F. Azough, R. Freer, M. Thrall, R. Cernik, F. Tuna, D. Collison, Microstructure and properties of Co-, Ni-, Zn-, Nb- and W-modified multiferroic $BiFeO_3$ ceramics, Journal of the European Ceramic Society 30 (2010) 727–736.
[6] X.L. Yan, J.G. Chen, Y.F. Qi, J.R. Cheng, Z.Y. Meng, Hydrothermal synthesis and characterization of multiferroic $Bi_{1-x}La_xFeO_3$ crystallites, Journal of the European Ceramic Society 30 (2010) 265–269.
[7] D.C. Arnold, K.S. Knight, F.D. Morrison, P. Lightfoot, Ferroelectric–paraelectric transition in $BiFeO_3$: crystal structure of the orthorhombic β phase, Physical Review Letters 102 (2009) 27602.
[8] C. Michel, J.M. Moreau, G.D. Achenbach, R. Gerson, W. James, The atomic structure of $BiFeO_3$, Solid State Communications 7 (1969) 701–704.
[9] J.D. Bucci, Bk. Robertso, W.J. James, The precision determination of the lattice parameters and the coefficients of thermal expansion of $BiFeO_3$, Journal of Applied Crystallography 5 (1972) 187–191.
[10] S. Vijayanand, M.B. Mahajan, H.S. Potdar, P.A. Joy, Magnetic characteristics of nanocrystalline multiferroic $BiFeO_3$ at low temperatures, Physical Review B 80 (2009) 064423.
[11] J. Liu, L. Fang, F.G. Zheng, S. Ju, M.R. Shen, Enhancement of magnetization in Eu doped $BiFeO_3$ nanoparticles, Applied Physics Letters 95 (2009) 022511.
[12] Y.H. Lin, Q.H. Jiang, Y. Wang, C.W. Nan, L. Chen, J. Yu, Enhancement of ferromagnetic properties in $BiFeO_3$ polycrystalline ceramic by La doping, Applied Physics Letters 90 (2007) 172507.
[13] P. Thakuria, P.A. Joy, High room temperature ferromagnetic moment of Ho substituted nanocrystalline $BiFeO_3$, Applied Physics Letters 97 (2010) 162504.
[14] S.M. Selbach, T. Tybell, M.A. Einarsrud, T. Grande, High-temperature semiconducting cubic phase of $BiFe_{0.7}Mn_{0.3}O_{3+delta}$, Physical Review B 79 (2009) 214113.
[15] I. Levin, S. Karimi, V. Provenzano, C.L. Dennis, H. Wu, T.P. Comyn, T.J. Stevenson, R.I. Smith, I.M. Reaney, Reorientation of magnetic dipoles at the antiferroelectric–paraelectric phase transition of $Bi_{1-x}Nd_xFeO_3$ ($0.15 <= x <= 0.25$), Physical Review B 81 (2010) 020103.
[16] J.B. Li, G.H. Rao, Y. Xiao, J.K. Liang, J. Luo, G.Y. Liu, J.R. Chen, Structural evolution and physical properties of $Bi_{1-x}Gd_xFeO_3$ ceramics, Acta Materialia 58 (2010) 3701–3708.
[17] H. Qin, H. Zhang, B.-P. Zhang, L. Xu, Hydrothermal synthesis of perovskite $BiFeO_3$–$BaTiO_3$ crystallites, Journal of the American Ceramic Society 94 (2011) 3671–3674.
[18] H.M. Zheng, F. Straub, Q. Zhan, P.L. Yang, W.K. Hsieh, F. Zavaliche, Y.H. Chu, U. Dahmen, R. Ramesh, Self-assembled growth of $BiFeO_3$–$CoFe_2O_4$ nanostructures, Advanced Materials 18 (2006) 2747–2752.
[19] J.B. Li, Y.P. Huang, G.H. Rao, G.Y. Liu, J. Luo, J.R. Chen, J.K. Liang, Ferroelectric transition of aurivillius compounds $Bi_5Ti_3FeO_{15}$ and $Bi_6Ti_3Fe_2O_{18}$, Applied Physics Letters 96 (2010) 222903.
[20] V.F. Freitas, L.F. Cotica, I.A. Santos, D. Garcia, J.A. Eiras, Synthesis and multiferroism in mechanically processed $BiFeO_3$–$PbTiO_3$ ceramics, Journal of the European Ceramic Society 31 (2011) 2965–2973.
[21] M.-S. Cao, W.-L. Song, Z.-L. Hou, B. Wen, J. Yuan, The effects of temperature and frequency on the dielectric properties, electromagnetic interference shielding and microwave-absorption of short carbon fiber/silica composites, Carbon 48 (2010) 788–796.
[22] Y.-J. Chen, G. Xiao, T.-S. Wang, Q.-Y. Ouyang, L.-H. Qi, Y. Ma, P. Gao, C.-L. Zhu, M.-S. Cao, H.-B. Jin, Porous $Fe_3O_4$/carbon core/shell nanorods: synthesis and electromagnetic properties, Journal of Physical Chemistry C 115 (2011) 13603–13608.
[23] M.S. Cao, X.L. Shi, X.Y. Fang, H.B. Jin, Z.L. Hou, W. Zhou, Y.-J. Chen, Microwave absorption properties and mechanism of cagelike $ZnO/SiO_2$ nanocomposites, Applied Physics Letters 91 (2007) 203110.
[24] X. Li, L. Zhang, X. Yin, Synthesis, electromagnetic reflection loss and oxidation resistance of pyrolytic carbon–$Si_3N_4$ ceramics with dense $Si_3N_4$ coating, Journal of the European Ceramic Society 32 (2012) 1485–1489.
[25] Y.A. Shevchuk, V.V. Gagulin, S.K. Korchagina, V.V. Ivanova, Dielectric properties of solid solutions based on ferroelectric–antiferromagnetic $BiFeO_3$ over the microwave range, Ferroelectrics 300 (2004) 101–106.
[26] F.B.A. Ahad, D.S. Hung, Y.D. Yao, S.F. Lee, C.S. Tu, T.H. Wang, Y.Y. Chen, Y.P. Fu, Dielectric constant at x-band microwave frequencies for multiferroic $BiFeO_3$ thin films, Journal of Applied Physics 105 (2009) 07D912.
[27] Z.-L. Hou, H.-F. Zhou, J. Yuan, Y.-Q. Kang, H.-J. Yang, H.-B. Jin, M.-S. Cao, Enhanced ferromagnetism and microwave dielectric properties of $Bi_{0.95}Y_{0.05}FeO_3$ nanocrystals, Chinese Physics Letters 28 (2011) 037702.
[28] W.L. Song, M.S. Cao, Z.L. Hou, X.Y. Fang, X.L. Shi, J. Yuan, High dielectric loss and its monotonic dependence of conducting-dominated multiwalled carbon nanotubes/silica nanocomposite on temperature ranging from 373 to 873 K in x-band, Chinese Physics Letters 94 (2009) 233110.
[29] Y.H. Lou, G.L. Song, F.G. Chang, Z.K. Wang, Investigation on dependence of $BiFeO_3$ dielectric property on oxygen content, Chinese Physics B 19 (2010) 077702.
[30] S. Ju, T.Y. Cai, First-principles studies of the effect of oxygen vacancies on the electronic structure and linear optical response of multiferroic $BiFeO_3$, Applied Physics Letters 95 (2009) 231906.
[31] J.T. Bendler, M.F. Shlesinger, Defect-diffusion models of relaxation, Journal of Molecular Liquids 36 (1987) 37–46.
[32] Z.L. Hou, M.S. Cao, J. Yuan, X.Y. Fang, X.L. Shi, High-temperature conductance loss dominated defect level in h-BN: experiments and first principles calculations, Journal of Applied Physics 105 (2009) 076103.

[33] S.S. Kim, S.B. Jo, K.I. Gueon, K.K. Choi, J.M. Kim, K.S. Churn, Complex permeability and permittivity and microwave-absorption of ferrote–rubber composite in x-band frequencies, IEEE Transactions on Magnetics 27 (1991) 5462–5464.

[34] P. Singh, V.K. Babbar, A. Razdan, R.K. Puri, T.C. Goel, Complex permittivity, permeability, and x-band microwave absorption of CaCoTi ferrite composites, Journal of Applied Physics 87 (2000) 4362–4366.

[35] W.L. Song, M.S. Cao, Z.L. Hou, J. Yuan, X.Y. Fang, High-temperature microwave absorption and evolutionary behavior of multiwalled carbon nanotube nanocomposite, Scripta Mater 61 (2009) 201–204.

[36] Z.L. Hou, L. Zhang, J. Yuan, W.L. Song, M.S. Cao, High-temperature dielectric response and multiscale mechanism of $SiO_2/Si_3N_4$ nanocomposites, Chinese Physics Letters 25 (2008) 2249–2252.